Journal of Colloid and Interface Science 605 (2022) 110–119

Contents lists available at ScienceDirect

Journal of Colloid and Interface Science

journal homepage: www.elsevier.com/locate/jcis

Polystyrene perturbs the structure, dynamics, and mechanical properties of DPPC membranes: An experimental and computational study

Davide Bochicchio [a], Laura Cantu [b], Maria Vittoria Cadario [b], Leonardo Palchetti [b], Francesca Natali [c], Luca Monticelli [d], Giulia Rossi [a,*], Elena Del Favero [b,*]

[a] Department of Physics, University of Genoa, Via Dodecaneso 33, 16146 Genoa, Italy
[b] Department of Medical Biotechnology and Translational Medicine, University of Milan, LITA V.le F.lli Cervi 93, 20090 Segrate, Italy
[c] Institut Laue-Langevin, 71 avenue des Martyrs, CS 20156, 38042 Grenoble Cedex 9, France
[d] IBCP, CNRS, UMR 5086, 7 Passage du Vercors, 69007 Lyon, France

GRAPHICAL ABSTRACT

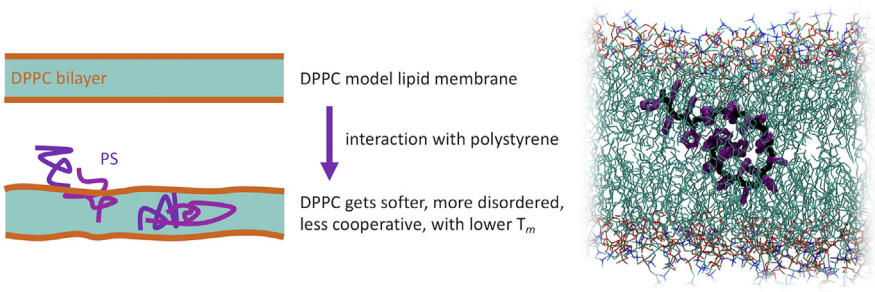

ARTICLE INFO

Article history:
Received 14 April 2021
Revised 16 June 2021
Accepted 9 July 2021
Available online 18 July 2021

Keywords:
Model membrane
Lipid bilayer
Polystyrene
X-ray scattering
Differential Scanning Calorimetry (DSC)
Elastic Neutron Scattering (ENS)
Molecular dynamics (MD)
Nanoplastics

ABSTRACT

Synthetic plastic oligomers can interact with the cells of living organisms by different ways. They can be intentionally administered to the human body as part of nanosized biomedical devices. They can be inhaled by exposed workers, during the production of multicomponent, polymer-based nanocomposites. They can leak out of food packaging. Most importantly, they can result from the degradation of plastic waste, and enter the food chain. A physicochemical characterization of the effects of synthetic polymers on the structure and dynamics of cell components is still lacking. Here, we combine a wide spectrum of experimental techniques (calorimetry, x-ray, and neutron scattering) with atomistic Molecular Dynamics simulations to study the interactions between short chains of polystyrene (25 monomers) and model lipid membranes (DPPC, in both gel and fluid phase). We find that doping doses of polystyrene oligomers alter the thermal properties of DPPC, stabilizing the fluid lipid phase. They perturb the membrane structure and dynamics, in a concentration-dependent fashion. Eventually, they modify the mechanical properties of DPPC, reducing its bending modulus in the fluid phase. Our results call for a systematic, interdisciplinary assessment of the mechanisms of interaction of synthetic, everyday use polymers with cell membranes.

1. Introduction

The undesired dispersion of micro and nanoplastics in the environment is one of the most challenging problems the scientific

* Corresponding authors.
E-mail addresses: rossig@fisica.unige.it (G. Rossi), elena.delfavero@unimi.it (E. Del Favero).

https://doi.org/10.1016/j.jcis.2021.07.069
0021-9797/

community and society as a whole have to face. Worldwide, we are approaching the yearly production of 400 million tons of plastics [1], and a considerable percentage of plastic products are disposable. While the problem of macroscopic plastic fragments is severe enough to harm terrestrial and ocean wildlife [2], the additional problem of micro- and nano-sized plastic fragments is more subtle but equally daunting [1,3–5]. When the plastic waste reaches the ocean, plastics is progressively degraded, its fragments are reduced in size by the effect of mechanical stress, solar radiation, bacteria, and oxidizing conditions [3]. Increasing evidence demonstrates that tiny plastic particles can enter the aquatic food chain, for instance via adsorption onto algae and subsequent ingestion by zooplankton or crustaceans [6]. In addition, nanoplastics are produced industrially for common products as cosmetics, nanocomposites, biomedical or formed during the mechanical breakdown of daily-use products [7]. The release of potentially toxic compounds from polymeric packaging materials of polystyrene into the contacted food is also of great importance for health-related impacts [8].

Given this picture, it is of fundamental importance to understand the degree of toxicity of micro- and nano-sized plastic. A few studies outlined that plastic nanoparticles can accumulate in living organisms' tissues (mussels, shrimps, and fish) and affect their metabolism [9–11]. It is also known that plastic nanoparticles' size plays an important role: smaller particles have a greater chance of penetrating and diffusing within the host organism's tissues [9]. Low molecular weight polymer chains can leach out of plastic objects stranded on the coasts and in seawater [12]. While it is clear that these micro- and nano-sized plastic particles can cause serious problems, little is known about the molecular details of their interaction with living cells.

One of the first barriers that plastic nanoparticles encounter when coming in contact with living organisms is the plasma membrane. Most of the every-day plastic consists of hydrophobic polymers, such as polystyrene (PS), polyethylene (PE), and polypropylene (PP). While long-chain polymers form stable solid phases, shorter chains form low-melting glasses and liquids [13,14] and can be mixed with organic solvents. Low molecular weight hydrophobic polymers are more likely to interact with the hydrophobic region of lipid membranes than with water, but the degree of damage or modification of the membrane properties that they can cause is not trivial to assess. A few years ago, our group started to tackle the problem from a computational point of view. In a first pioneering study, we investigated the interaction between polystyrene nanoparticles and single-component phospholipid membranes [15]; we predicted that polystyrene nanoparticles easily penetrate the hydrophobic core of lipid membranes and affect their structural and mechanical properties. In a following study, we compared the effect of PS to that of two other common hydrophobic polymers, PE and PP [16]. We found that the interaction of polymers with membranes depends crucially on polymer structure, chain length, and aromaticity. These computational studies proposed a molecular mechanism of interaction between hydrophobic polymers and model lipid bilayers, but they lacked a direct experimental verification. Furthermore, given the high computational cost of studying the polymer-membrane interaction over the relevant length and time scales, those studies were carried out at the coarse-grained level, using the Martini force field [17] for the description of both polymers and lipids. While those coarse-grained models were carefully validated in bulk solvents, questions on the models' accuracy should be addressed via comparison with more detailed atomistic models and experimental data.

The rare existing experimental literature shows that PS monomers and very short oligomers can be included in amphiphilic bilayers, synthetic or biomimetic, with an impact on their organization [18]. Only very recently, an experimental study has appeared showing that very short PS oligomers (5-mers) can alter the ability of admixed natural saturated and unsaturated lipids to form distinct domains with different fluidities in the hosting model membrane [19].

In the present work, we overcome the recalled crucial issues and present a combined experimental and computational investigation of the interaction of PS nanoplastic with dipalmitoylphosphatidylcholine (DPPC) lipid bilayers, focusing on the effects of the introduction of short PS chains (PS25, 25-mers) on the structural, thermodynamic and mechanical properties of DPPC membranes. We use parallel Differential Scanning Calorimetry (DSC) as well as small and wide angle x-ray scattering experiments (SAXS and WAXS) to assess the structural properties of DPPC/PS bilayers at different temperatures. The local dynamics of the membranes in the longitudinal and cross direction is experimentally accessed by elastic neutron scattering (ENS). At the same time, we use computer simulations (Molecular Dynamics, MD), with an atomistic resolution, to investigate the molecular details of the interactions between PS and DPPC and their effect on the mechanical properties of the bilayers. Our combined experimental and computational approach tackles the problem at different time and length scales and demonstrates that PS has major effects on the architecture, dynamics, and cooperativity of DPPC bilayers.

2. Results and discussion

We investigate model membrane systems in aqueous solutions. Polystyrene (MW 2500, PS25)/DPPC mixed bilayers were prepared and modeled with a PS/DPPC mass fraction in the 0–15%. While these concentrations are large as absolute values, they may be representative of the local adsorption of plastics nanoparticles within a cell membrane. Experimentally, the PS/DPPC mixed bilayers were prepared by the thin-film hydration method. Multilamellar mixed PS25/DPPC/water systems prepared at c = 20 mg/ml are observed by differential scanning calorimetry (DSC) or let to sediment to a final "maximum swelling" (about 54% volume fraction) to be observed by SAXS and WAXS experiments [20]. Similar solutions prepared at c = 50 mg/ml were let to sediment on silicon wafers and dehydrate to form highly oriented membranes stacks and observed by ENS experiments.

2.1. Thermal properties

2.1.1. DSC measurements

Fig. 1 reports the upward calorimetric scans of PS25/DPPC bilayers at increasing PS volume fraction (0–15%). We focus on the evolution of two typical endothermic peaks, associated with the pre-transition (at temperature T_p) and the main transition (at temperature T_m), the latter corresponding to the gel-to-fluid transition of the lipid chains. The presence of PS25 affects both T_p and T_m and reduces the associated enthalpies (Fig. 1b). T_p decreases from 35 °C to 33.9 °C upon PS25 increase until 10% PS mass fraction, with a 60% reduction of the associated ΔH_p. In the same range of PS25 content, T_m also lowers from 41.25 °C to 41 °C, and the presence of polystyrene reduces the associated ΔH_m values.

Thermograms in Fig. 1 also show that the presence of PS25 induces a broadening of the main phase transition of DPPC. This melting transition's cooperativity is estimated by the value of the cooperative unity C.U., obtained by the ratio between the van't Hoff enthalpy ΔH_{vH} and the measured ΔH_m. The van't Hoff enthalpy is calculated according to the equation $\Delta H_{vH} \cong 6.9\ T_m^2/\Delta T_{1/2}$, where $\Delta T_{1/2}$ is the full width at half the maximum of the calorimetric peak [21]. The evolution of the C.U. is reported in Fig. 1c, showing

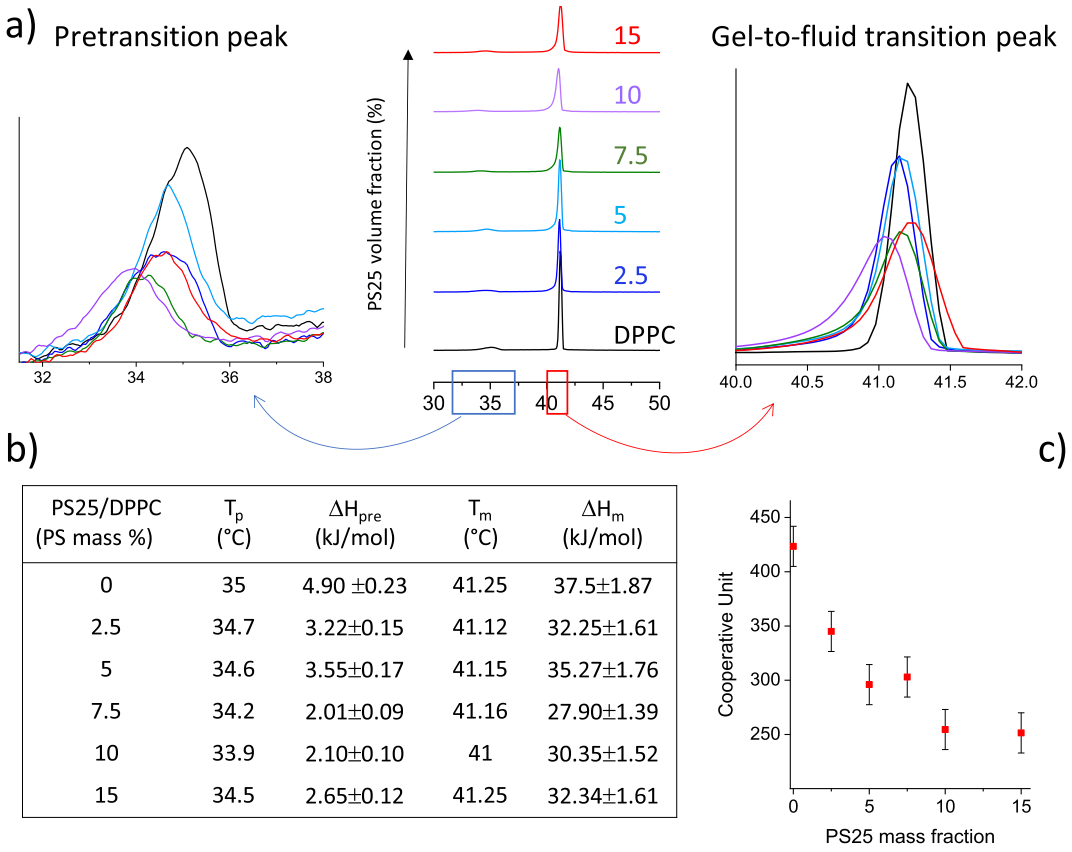

PS25/DPPC (PS mass %)	T_p (°C)	ΔH_{pre} (kJ/mol)	T_m (°C)	ΔH_m (kJ/mol)
0	35	4.90 ±0.23	41.25	37.5±1.87
2.5	34.7	3.22±0.15	41.12	32.25±1.61
5	34.6	3.55±0.17	41.15	35.27±1.76
7.5	34.2	2.01±0.09	41.16	27.90±1.39
10	33.9	2.10±0.10	41	30.35±1.52
15	34.5	2.65±0.12	41.25	32.34±1.61

Fig. 1. DSC. (a) Calorimetric upward thermograms of PS25/DPPC multilamellar systems at increasing PS25 mass fraction, from bottom to top 0%-15%. Left insert: zoom on the pretransition region, same colour code as for the data. Right insert: zoom on the main transition region, same colour code as for the data. (b) Pretransition T_p and gel-to-fluid main transition T_m temperatures (peak positions in the inserts of Panel a)) and associated enthalpies ΔH_p and ΔH_m. c) Calculated cooperative unit C.U. for the main transition as a function of PS25 mass fraction.

a progressive decrease of cooperativity upon PS25 increase, reaching a plateau at 10% PS25 mass fraction.

Notably, as seen in Fig. 1, at 15% PS25 content, the melting temperature T_m abruptly rises back to 41.25 °C, recovering that of pure DPPC, although with a smaller cooperative unit, C.U. This behavior suggests that local segregation of PS25 chains within the bilayer may occur, above a critical concentration between 10% and 15%, fencing regions where pure DPPC is present. Such a compositional inhomogeneity might affect the membrane even out of the order-disorder transition regime. To reinforce this finding, we explored the effect of PS90, a longer PS polymer with 90 styrene groups, on DPPC membranes. DSC experiments show that at 5% volume fraction, the effect of PS90 is very similar to the one found for PS25; both the pretransition and the main transition shift to lower, and similar, temperatures, namely T_p = 34.7 °C (T_p = 34.6 °C for PS25), and T_m = 41.18 °C (T_m = 41.15 °C for PS25). Differently, at 10% PS volume fraction, the further substantial drop of the transition temperatures induced by the short-chain PS25 is not observed for the long-chain PS90: T_p = 33.9 °C (PS25), T_p = 34.5 °C (PS90) and T_m = 41.00 °C (PS25), T_m = 41.18 °C (PS90). These results indicate that the threshold concentration for a putative effective local segregation of PS from DPPC is lower for the longer PS90 chains (lower than 10% volume fraction).

Overall, our calorimetric data show that the insertion of PS into DPPC lipid bilayers promotes the stabilization of the fluid lipid phase and reduces the system's cooperativity in a dose-dependent fashion. Moreover, above a threshold concentration, it appears to promote lateral phase separation within the DPPC bilayer, with an inhomogeneous lateral distribution of PS in the membrane.

2.2. Structural properties

2.2.1. SAXS and WAXS measurements

In order to investigate the effect of PS25 on the multiscale structure of DPPC membranes as they evolve across different lipid phases, we performed parallel DSC and SAXS/WAXS experiments in multilamellar systems as the temperature was raised from 25 to 55 °C (experimental details are reported in Section 4). Fig. 2a reports compared experimental data on DPPC, and PS25/DPPC (5% PS25 mass fraction) focused on the small angle range. The typical phase behavior of multilamellar systems can be identified in both cases. The mesoscale structure changes at the pretransition and main transition temperatures, T_p and T_m, as indicated by the parallel DSC thermograms reported vertically on the left-hand side, with the same temperature scale, coupling thermotropic and thermodynamic information. The pretransition marks the structural change from the $L_{\beta'}$ lamellar gel phase, characterized by tilted acyl chains, to the $P_{\beta'}$ phase, characterized by the presence of periodic ripples on the membrane's surface [22–24].

Structural differences between the two lamellar systems on all length-scales, down to the lipid chain packing, can be appreciated by looking at the x-ray spectra recorded in an extended SAXS/WAXS q-range, 0.09 – 20 nm^{-1}, and compared at the same temperature. Fig. 2b compares spectra at various points during the temperature scan, i) deep in the gel phase, ii) at the pretransition, iii) at the main transition, and iv) deep in the fluid phase.

i) At T = 25° C, both systems are in the $L_{\beta'}$ phase. The equally spaced intensity peaks, in the SAXS region, at q = 0.99, 1.98, 2.97, 3.96, 4.95, correspond to a lamellar repeat D spac-

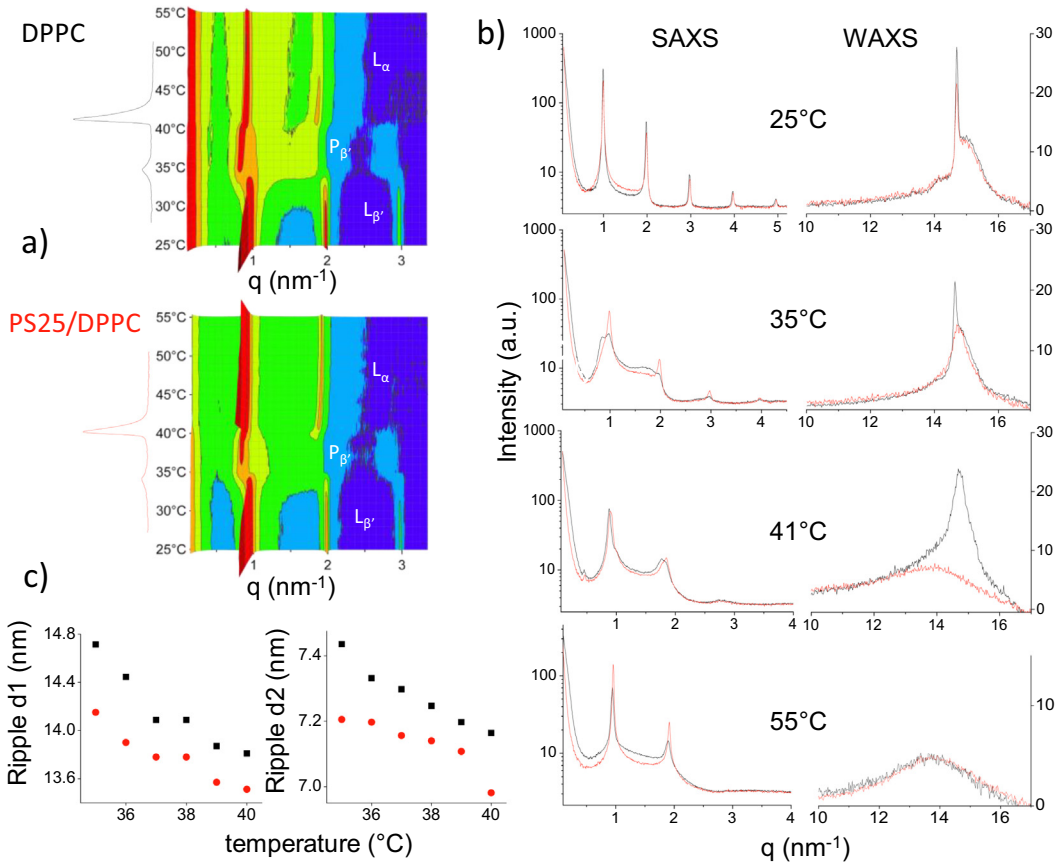

Fig. 2. Small and wide angle x-ray scattering (SAXS and WAXS) on DPPC (black lines and symbols) and PS25/DPPC (red lines and symbols). a) SAXS intensity patterns during a temperature scan from 25 °C to 55 °C (scan rate 1 °C/min). Simultaneous thermograms are reported vertically on the left with the same temperature scale, coupling thermotropic and thermodynamic information. b) Intensity profiles in the SAXS (left) and WAXS (right) regions of the two multilamellar systems in the $L_{\beta'}$ phase (T = 25 °C), at the two boundaries of the $P_{\beta'}$ ripple phase (T = 35 °C, T = 41 °C), in the Lα fluid lamellar phase (T = 55 °C). c) Characteristic distances in the ripple phase as calculated from the intensity peaks' position: d1 = 2π/q1 and d2 = 2π/q2.

ing of 6.3 nm, as expected for DPPC [25]. Only a very slight shift to higher q-values (shorter distances) occurs in the presence of a 5% volume fraction of PS25. The WAXS diffraction patterns show the asymmetric double Bragg peak typical of the orthorhombic packing of tilted chains occurring in the $L_{\beta'}$ phase [26]. DPPC molecules have an interfacial area of 48 Å^2 and tilted gel chains (θ = 31°) packed in the hydrophobic layer, 17.3 Å thick.

ii) The spectra taken at T = 35 °C confirm that the presence of PS25 anticipates the pretransition from the $L_{\beta'}$ to the $P_{\beta'}$ phase to lower temperatures. While pure DPPC still shows the orthorhombic order of the $L_{\beta'}$ phase, the system doped with PS25 has already turned its lipid chain packing (WAXS region) to the hexagonal order, with one single characteristic Bragg peak.

iii) The structural effect due to PS25 also appears in the main transition process. At T = 41 °C, both pure and PS-doped systems display the ripple phase's typical pattern on the mesoscale (SAXS range). Nonetheless, on the local scale (WAXS range), DPPC shows up with the hexagonal Bragg peak (q = 14.7 nm^{-1}), while the PS25/DPPC system already features a broad structure peak (at q = 13.9 nm^{-1}), revealing that the melting transition of lipid chains has already occurred. Indeed, this broad structure peak is distinctive of the lipid chains' fluid arrangement, as in the Lα fluid phase [27].

iv) Finally, at T = 55 °C, in the L_α fluid phase, the lipid chains reach a similar local packing, giving rise to the WAXS structure peaks observed at the same position, q = 13.8 nm^{-1}, corresponding to a characteristic distance d_c = 4.55 Å. Meanwhile, the mesoscale arrangement (SAXS range) shows that a minor shrinking is induced by PS25, similar to what was observed at low temperature and corresponding to a shorter lamellar repeat D spacing, 6.56 nm instead of 6.68 nm.

Our parallel experiments reveal that the influence of PS on membrane structure extends beyond the transition processes' modulation, being also displayed in the $P_{\beta'}$ ripple phase that occurs in between the two transition events. We recall that, as a distinctive feature, the $P_{\beta'}$ intermediate phase is affected by inhomogeneities in the thickness and mean interfacial area of the bilayer. Our experimental data for pure DPPC, namely, the observed intensity peaks' positions and the lattice parameters calculated from the diffraction pattern (see Supplementary material), are in perfect agreement with previous studies at the same temperature [24,28]. The architecture of DPPC on the mesoscale can be modeled as a stack of rippled bilayers, identified by two lattice parameters; the ripple repeat in the membrane plane (d1), connected to the distance between two parallel corrugations, and the bilayer repeat (d2), connected to the lamellar repeat spacing along the lamellar stack. Such rippled geometry originates from

the creation of one-dimensional parallel fluid line-defects in a gel bilayer due to the competition between headgroup ordering, favored by elastic forces, and headgroup hydration [22]. In the $P_{\beta'}$ ripple phase of DPPC, the growth of these defects leads to an asymmetric sawtooth profile of the bilayers, with a short thinner arm half the length of the thicker one [24,29]. Simulations from a previous study showed that lipids in the kink regions between the two arms are highly disordered and mobile [30].

Our data (Fig. 2, Panel c) show that the presence of PS25 forces a notable reduction in both characteristic distances all over the ripple phase domain. PS increases the surface density of corrugations on the membrane and helps the occurrence of kink regions (smaller d1). We speculate that polystyrene chains may act as structural defects increasing the inhomogeneity distributed within the lipid bilayer, similarly to fluid lipid line defects. Also, the distance between the bilayers is slightly shorter in the presence of PS25 (smaller d2), a difference that amounts to ~0.2 nm in the low-temperature region of $P_{\beta'}$, and progressively fades as the high-temperature edge of the ripple phase is approached, where the transition to the fluid phase occurs. The sudden drop of the inter-bilayer (d2) repeat at T = 40 °C is likely due to the anticipated occurrence of the main transition in PS25/DPPC bilayers. Notably, the short-scale and meso-scale structural features of the PS-doped bilayers do not show the usual coupling found in phospholipid bilayers. At T = 41 °C, the mixed PS25/DPPC bilayers, although already showing on the local-scale pattern of fluid disordered lipid chains (Fig. 2b) WAXS), still keeps the ripple architecture on the mesoscale (Fig. 2b) SAXS), possibly sustained by the disposition of polystyrene chains along the line defects. This point has been further investigated by molecular dynamics simulations (see later on). Eventually, at a higher temperature and after a suitable delay, the bilayer flattens, as expected in the L_α fluid phase.

2.2.2. Molecular dynamics simulations

To investigate in a more detailed way and with a molecular resolution the behavior of PS25 chains inside DPPC bilayers, we performed molecular dynamics (MD) simulations. In this study, all the simulations are performed at the united atom level (OPLS-UA force field [31] and Berger lipids [32], see Section 4 for further details). We constructed three systems, composed of a DPPC lipid bilayer and 5%, 10%, or 15% of PS25 chains. We randomly dispersed the PS25 chains in the bilayer, locally minimized, and equilibrated the system for 50 ns. Then we performed 2 μs production runs at a temperature of 57 °C in NPT conditions for each system. The temperature has been chosen to have the lipids in the fluid phase, allowing the spontaneous rearrangement of PS25 chains within reasonable simulation times (hundreds of ns).

PS chains conformation and location within the membrane. At 5% and 10% of mass ratio, PS25 chains are compact and, on average, spherical objects buried inside the hydrophobic core of the DPPC bilayer (see Fig. 3a, top). PS25 chains are confined to the center of DPPC bilayers, as shown by the density profiles of PS25 along z (Fig. 3a, bottom). The sphericity of the single chains can be evaluated by looking at the radii of gyration about the x-, y- and z-axes. In particular, given the symmetry of the system, we distinguish between an in-plane ($(Rg_x + Rg_y)/2$) and an out-of-plane (Rg_z) component. The results at 5% and 10% of mass ratios are comparable: both components measure on average 0.71 +/- 0.03 nm (see Figure S3). In these simulations, the PS25 chains diffuse along the membrane plane at both PS mass ratios, remaining dissolved into the hydrophobic core and showing no aggregation signs (See Fig. 3b, first two snapshots). However, the behavior of polystyrene changes when its concentration is further increased. At 15% of mass ratio, PS25 chains collapse to form a single aggregate (see Fig. 3b, last snapshot). Once formed (after ~100 ns), the aggregate, despite being dynamical and liquid-like, is stable for the whole simulation run. PS25 chains belonging to the aggregate are less globular than the dissolved PS25 chains: they become slightly elongated in the out-of-plane direction, as demonstrated by Rg_z becoming higher than in the other systems (0.83 +/- 0.03 nm, see Figure S3). We quantified this concentration-dependent aggregation behavior by analyzing the number of contacts between atoms of the polymers and atoms of the lipids (see Fig. 3c). At 5% and 10% of mass ratios, the number of mixed contacts remains essentially

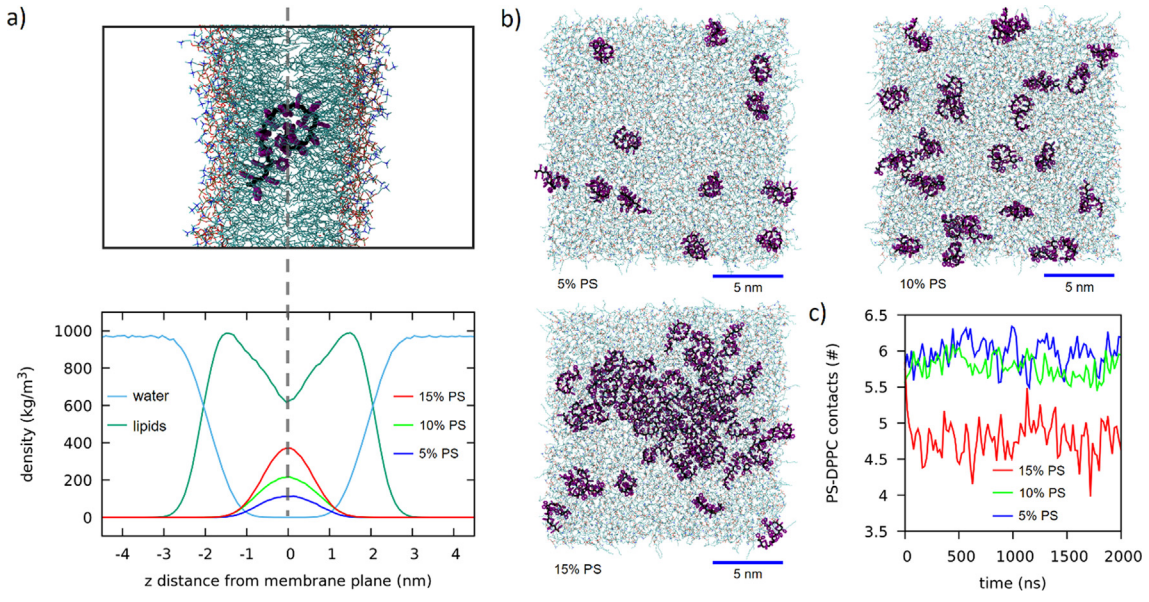

Fig. 3. The behavior of PS25 chains in DPPC bilayers at different concentrations. (a) Top: typical configuration of a single PS25 chain dissolved into the hydrophobic core of the DPPC bilayer. The carbon chain is in black, while phenyl groups are in purple. Water is not shown for clarity. Bottom: density profiles along the axis perpendicular to the membrane plane from the simulations with 0%, 5%, 10%, and 15% of PS25. The densities of water (cyan) and lipids (dark green) are taken from the pure DPPC simulation (0%), while the density of PS25 is in blue for 5%, in green for 10%, and in red for 15% mass concentration. (b) Top view of representative snapshots taken from a DPPC bilayer's simulations containing 5%, 10%, and 15% of PS25 chains. (c) The normalized number of contacts between PS25 atoms and DPPC atoms as a function of time. The contacts were normalized by dividing the total number of contacts by the number of polystyrene atoms (the number of lipids is the same in the three systems).

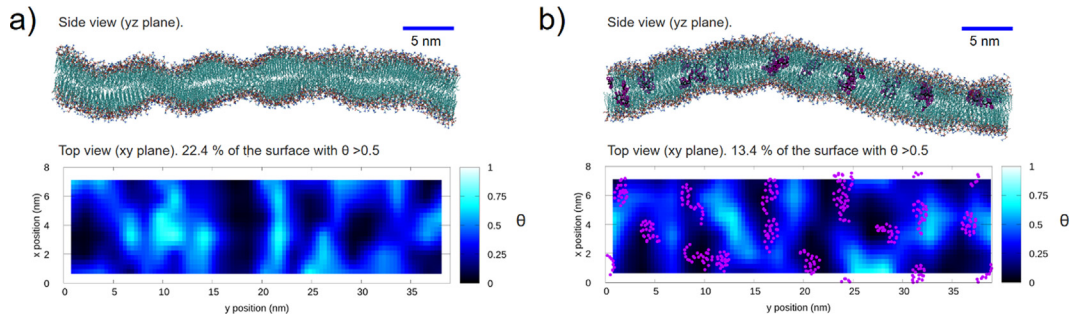

Fig. 4. Effect of PS25 chains on the ripple phase (measured from simulations at 17° C). (a) Snapshot from the pure DPPC asymmetric system and 2D map of the order parameter θ for the same system. (b) Snapshot from the asymmetric system with 5% of PS25 chains and 2D map of the order parameter θ for the same system. Purple points on the map represent the average position of the PS25 residues in the time interval in which θ has been measured.

constant, while at 15% there is a fast decrease at the beginning of the run: the signature of aggregation. We verified the reliability of this result by running three additional independent simulations (500 ns for each run), and we obtained comparable results (see Figure S4).

The concentration-dependent aggregation of PS25 in the DPPC membrane confirms our experimental data, providing a molecular interpretation of the concentration-dependent thermal properties of the DPPC/PS25 mixture revealed by DSC. Indeed, both phase transitions temperatures tend to decrease up to 10% of PS25 volume fraction, but the DPPC behavior is recovered at 15% PS25 concentration, except for the cooperative unit C.U. Combined results suggest partial segregation of PS chains within the bilayer above a critical concentration, which is between 10% and 15% for PS25 according to both simulations and experiments. Aggregation of hydrophobic chains in the interior of lipid membranes is analogous to the nucleation of lipid droplets, observed in simulations [33] and experiments [34] upon addition of oil (e.g., triglycerides) to lipid bilayer membranes or even cell membranes [35]. Both phenomena can be described as a type of liquid–liquid phase separation, taking place when the concentration of the hydrophobic chains increases above a certain threshold.

Effect of PS25 on the ripple phase. We used MD simulations to investigate how the presence of PS25 chains can affect the ripple phase features. We created a pure DPPC bilayer ribbon, as shown in Fig. 5, with and without 5% of PS25 chains. The system temperature was decreased in 100 ns from 57 °C to 17 °C and then equilibrated at 17 °C for 400 ns (see Section 4 for further simulation details). As shown in Fig. 4a, after 500 ns, the pure DPPC membrane presents alternating ordered and disordered phases, with a sawtooth profile in some regions that resembles a ripple phase profile. We analyzed the alternance of ordered and disordered phases by constructing a 2D map of an *ad hoc* order parameter, θ, which measures lipid tails' elongation by analyzing their dihedral angles (details about the calculation of θ are provided in the Section 4). θ can theoretically vary from 0 (in regions containing only *cis* dihedrals) to 1 (in regions containing only *trans* dihedrals).

When PS25 is present (Fig. 4b), the membrane profile is more homogeneous. Looking at the 2D map of the order parameter, it becomes clear that the ordered phase is hindered in the regions of the membrane incorporating PS25 chains. Indeed, white/cyan regions (high θ) are essentially polymer-free, while regions near the polymer are black/blue (low θ). We calculated for both systems (pure and with 5% of PS25) the fraction of the membrane surface presenting an order parameter θ > 0.5, obtaining 22.4% for the pure system and 13.4% for the hybrid system. These results highlight that the presence of 5% PS25, while allowing an alternation of ordered and disordered phases, on average has a disordering effect. We repeated the simulations and the analysis at a higher temperature (23° C). While both the pure and mixed systems appear much less ordered, the system containing PS25 chains is once again the least ordered (see supplementary Figure S5). These simulation results are consistent with the experimental data, showing that the repeat distances in the ripple phase are decreased in the presence of PS25 chains, putatively reflecting the increase of the fluid domains and the smoothing of the bilayer profile.

2.3. Local lipid dynamics and whole membrane mechanical properties

2.3.1. Neutron scattering experiments

Lipid dynamics. The local motion (at a tenth of nm scale) of the molecular groups within the membrane was assessed by neutron scattering elastic neutron scattering (ENS) experiments on highly oriented stacks of DPPC membranes, pure and doped with 5% PS of two different lengths (PS25 and PS90), as a function of temperature, from deep freeze (dampened motion) up to the gel-to-fluid transition. In order to discriminate between in-plane and out-of-plane dynamics, the oriented samples were tilted at 135 and 45°, respectively, with respect to the incoming neutron beam. Details are reported in the Section 4 and in the Supplementary Material. From the spectra of the elastic scattered intensity, the mean-square amplitude of atomic displacements (MSD) was calculated (see Section 4 for the details).

Fig. 5a shows the temperature dependence of the measured in-plane (MSD_{xy}) and out-of-plane (MSD_z) mean square displacement for pure DPPC and PS-doped samples. In both directions, a smooth increase ends up with an abrupt enhancement of the dynamics across the gel-to-fluid phase transition, occurring at T > 330 K, higher than expected for dispersed DPPC membranes, and is commonly observed in similar experiments on stacks of thousands of bilayers at low hydration [36]. From the slope of MSD versus temperature below the phase transition, the associated force constant $\langle k' \rangle$ (the *resilience* or rigidity of the molecules [37]) in the gel phase is calculated (see eq.2 in the methods section) and reported as histograms in Fig. 5a. The dynamics for the pure DPPC membranes is clearly anisotropic, suggesting higher rigidity for the out-of-plane lipid motions as compared to the in-plane ones. The presence of 5% polystyrene, both PS25, and PS90, clearly reduces motional anisotropy; namely, it lowers the out-of-plane effective force constant, leading to enhanced molecular mobility in the cross direction of the membrane.

2.3.2. Molecular dynamics simulations

Lipid dynamics. We calculated the in-plane diffusion coefficient of DPPC lipids, as detailed in the Section 4 section. The results, summarized in Table 1, show a clear trend, with the lipid diffusion coefficient increasing from 0% to 15% of PS25 mass ratio. However,

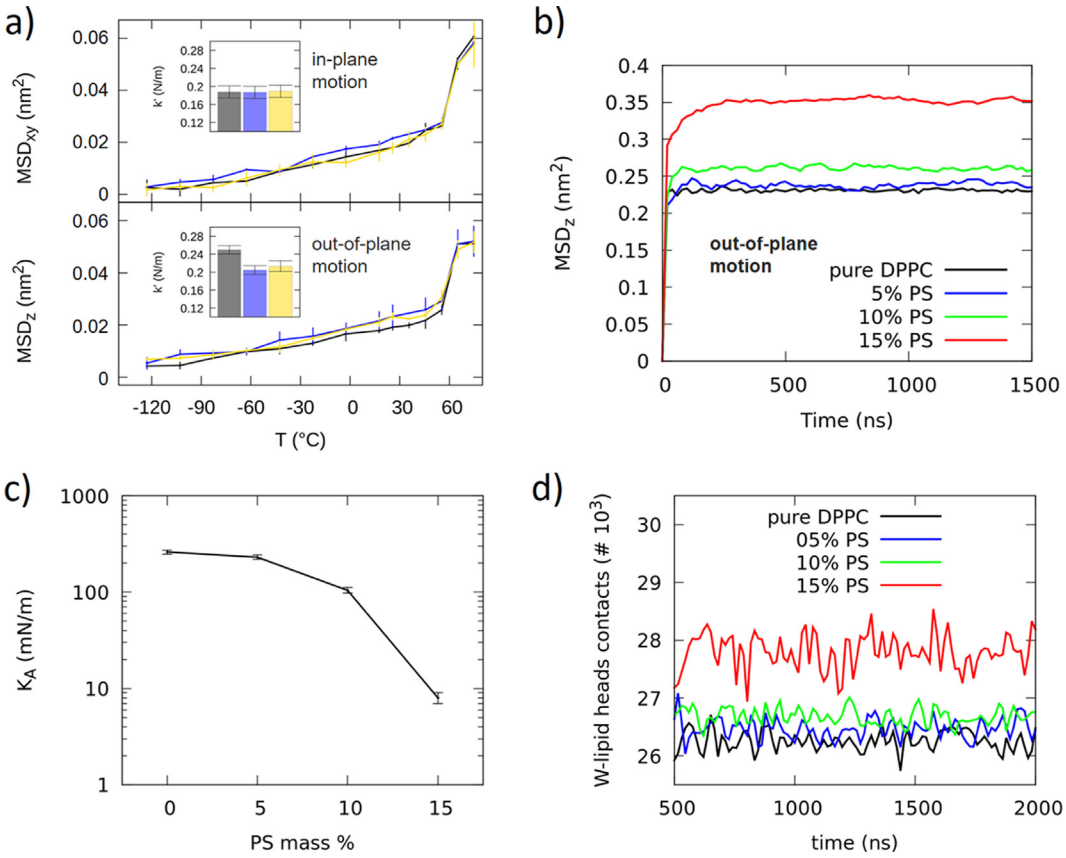

Fig. 5. Effect of PS25 chains on the dynamical and mechanical properties of DPPC bilayers. (a) Elastic neutron scattering experiments results. MSD calculated for the in-plane (135°, upper panel) and out-of-plane (45°, lower panel) motions, with corresponding force constants in insets. Black: pure DPPC; blue: PS25/DPPC; gold: PS90/DPPC. (b) Mean squared displacement along the axis perpendicular to the membrane plane as a function of time for the different PS25 mass ratios, calculated from MD simulations. (c) Area compressibility modulus as a function of the percentage of PS25 chains inside the DPPC bilayer, calculated from MD simulations. (d) Hydration of the lipid heads in MD simulations: number of contacts between lipid head atoms and oxygen atoms belonging to water molecules.

Table 1
Lateral diffusion coefficient of DPPC lipids, in the plane of the membrane, as a function of the PS25 mass percentage.

	Diffusion coefficient (cm^2/s)
0% (pure DPPC)	$1.2\ 10^{-7}$ ($\pm 0.1\ 10^{-7}$)
5% of PS25	$1.3\ 10^{-7}$ ($\pm 0.1\ 10^{-7}$)
10% of PS25	$1.4\ 10^{-7}$ ($\pm 0.1\ 10^{-7}$)
15% of PS25	$5.4\ 10^{-7}$ ($\pm 0.2\ 10^{-7}$)

the effect is not linear, becoming more pronounced at 15%. We further analyzed the dynamic properties of DPPC lipids in the presence of PS25 chains calculating the out-of-plane mean squared displacement of lipids (MSD_z, see Fig. 5b). The MSD_z too, increases with increasing PS25 mass ratio (from 0% to 15%). Despite being measured in the liquid phase and thus also with a different hydration, this increase is qualitatively coherent with ENS experimental measurements of the lipids out-of-plane MSD in the temperature range 250–330 K (below the lipid main transition for DPPC stacks).

Mechanical properties. A higher out-of-plane MSD is expected to be correlated with a modification of the mechanical properties of the whole bilayer [38]. Indeed, coherently with what was observed in our previous study with a coarser model [15], PS has a mechanical softening effect. We calculate the area compressibility modulus K_A for the bilayers at the three different concentrations and for a pure DPPC bilayer (see Fig. 5c). The K_A modulus progressively decreases with increasing the concentration of PS25 from 0% to 15%. There is a jump of one order of magnitude at 15%, indicating that the effect of aggregated chains on the membrane lateral rigidity is stronger than the effect of dispersed chains. Indeed, when measuring K_A for a phase-separated system, we effectively measure the compressibility of the softer phase (which in this case is a lipid-polymer mix with a very high local concentration of PS). This effect is analogous to previous predictions by MD simulations in lipid binary and ternary mixtures [39] and consistent with experimental observations on DMPC/DSPC mixtures [40]. It is also coherent with the strong increase in DPPC diffusion coefficients at 15% of PS25 mass ratio. We further analyzed the systems by looking at the degree of hydration of lipid heads (see Fig. 5d). While the effect of the polymer on the average hydration is minor at 5% and 10% of PS25 mass ratio, at 15% the hydration of lipid heads is significantly enhanced. This result, coherent with the increase in the average area per lipid (see Figure S6), provides a molecular-level interpretation of the results on the area compressibility modulus: when the PS25 chains aggregate concentrating in a specific region, there they cause a significant increase in lipid head group hydration, making the membrane softer.

We performed additional simulations to calculate the effect of 10% of PS25 on the bending modulus K_b of the DPPC bilayers. For details about the computational technique used to calculate K_b (buckling method) see Section 4. We only analyzed simulations with PS25 concentration below the aggregation threshold, because the theory underlying bending modulus calculations is only valid for homogeneous materials (https://doi.org/10.1063/1.4808077). The results are summarized in Table 2. The bending modulus of the pure DPPC membrane is in agreement with values from the

Table 2
Bending modulus of the pure DPPC bilayer and of a DPPC bilayer with 10% of PS25, calculated from MD simulations with the buckling technique.

	Bending modulus (k_BT)
0% (pure DPPC)	26.1 (± 1.0)
10% of PS25 (SIM1)	16.2 (± 2.8)
10% of PS25 (SIM2)	19.7 (± 3.4)

literature [39,41], while it decreases in the presence of polystyrene. The effect is substantial since at 10% of mass ratio the bending modulus is reduced by about one-third. Therefore, we can conclude that polystyrene chains significantly soften DPPC membranes, reducing both K_a and K_b.

3. Conclusions

With this study we clarified the effects induced by doping doses of nano-plastics made of a common industrial polymer, polystyrene, on the structure, dynamics, and mechanical properties of DPPC membranes. Thanks to the combination of diverse experimental and computational techniques, we could characterize the system at different time and length scales, reaching a clear and complete picture of the perturbations on the membranes.

United-atom simulations confirm that short polystyrene chains (25 monomers) incorporated within the DPPC lipid bilayer, tend to be hosted in hydrophobic core. Experimental DSC data show that nano-sized PS, once embedded in the DPPC lipid bilayer core, downshifts both the pre-transition and main transition temperature of DPPC, stabilizing the lipid fluid phase while reducing the system cooperativity in a dose-dependent fashion. However, the same data suggest that, above a threshold concentration of nanoplastic, the system undergoes partial phase separation. This behavior was clarified by unbiased molecular dynamics simulations, showing aggregation of PS chains only above 10% of PS mass fraction, consistent with the experiments.

Parallel SAXS and WAXS measurements revealed that the influence of PS extends beyond phase transition modulation, influencing structural features of the different phases. Interestingly, the presence of PS appears to be relevant for the Pβ' ripple phase that is observed between the two transition events, increasing the surface density of kinks. Once again, molecular dynamics simulations provide an interpretation at the atomic level: the formation of the ordered phase is hindered in the proximity of PS25 chains. While allowing the alternation of ordered and disordered phases typical of the ripple phase, on average, polystyrene has a disordering effect, effectively increasing the number of disordered regions. The fact that PS alters the ripple phase suggests that, more generally, it may have an impact on the border areas between different lipid phases. In this respect, the recent experimental finding that PS oligomers have an impact on phase coexistence of mixed lipid systems, has suggested that PS might interfere with cell membrane domain formation.

Furthermore, we showed that dynamic and mechanical properties of DPPC bilayers are perturbed. ENS experiments on highly oriented stacks of DPPC membranes indicated that polystyrene leads to enhanced lipid mobility in the direction of the membrane normal. Simulations confirm this effect. The effect of the presence of PS on the local lipid dynamics in a small environment within the model membrane, can be common to lipids embedded in different types of real, more complex membranes.

We also used molecular dynamics to calculate the mechanical properties of DPPC bilayers in the presence of PS. Coherently with previous studies performed with coarser computational models, we show that polystyrene softens the lipid membrane, significantly reducing its area compressibility modulus and bending modulus.

Our results suggest that the potential harm caused by the incorporation of nanoplastics should not be underestimated. In the case we analyzed, the nanoplastics concentration plays a major role in determining the extent of membrane perturbation.

Our study considers a model situation in which polymer chains are not covered by the organic and inorganic molecules that crowd natural water environments, and that may change the physicochemical nature of the nanoplastics-bio interface. Indeed, the formation of a biocorona [42], constituted by natural organic matter, protein-rich aquatic exudates, and other biomolecules, can modify the toxicity of nanoparticles, similarly to what happens *in vitro* and *in vivo* with protein coronas [43]. From this point of view, our results call for future investigation of the effects of more realistic plastic nanoparticles.

Another relevant issue that remains to be explored is the possible effect of nanoplastics membrane incorporation on membranes of more biologically relevant composition. In particular, membrane proteins are known to be sensitive to membrane elastic properties; changes in membrane elasticity may alter conformational equilibria, and therefore functioning, in membrane proteins [44,45].

Both these achievements, which can be accomplished by consolidating interdisciplinary, multi-approach experimental and computational protocols, would be fundamental steps to extend our understanding of the effect of nanoplastics on living organisms.

4. Materials and methods

Sample preparation. 1,2-dipalmitoyl-*sn-glycero*-3-phosphocholine (DPPC; synthetic, purity > 99%) was from Avanti Polar Lipids. Polystyrene for molecular weight standard (MW 2500 and 9000) was purchased from Merck Life Science. Multilamellar mixed DPPC + polystyrene (PS) systems were prepared by thin-film hydration method. Proper amount of each component were dissolved and mixed in chloroform at c < 1 mg/ml. After complete solvent removal in a rotating evaporator and under vacuum, the obtained lipid thin film was humidified, rehydrated (c = 20 mg/ml) and submitted to a freeze and thaw homogenization protocol. For dynamical experiments highly oriented membranes stacks were Supported membrane multistacks were obtained by deposition of 1.5 ml of a multilamellar solution (100 mg/ml) on three Si wafers (30 mm × 40 mm). After drying under humidity controlled conditions the sample was sealed in a flat aluminium cell.

Differential scanning calorimetry (DSC). Differential scanning calorimetry (DSC) experiments were performed with a MASC instrument [46]. Multilamellar solutions (0.2 ml) at c = 20 mg/ml were put in sealed glass capillaries and submitted to subsequent temperature cycles in the temperature range 25 °C < T < 55 °C at a scan rate of 0.33 °C/min.

Small and Wide Angle X-ray scattering (SAXS and WAXS). SAXS and WAXS experiments were performed at the SAXS beamline of Elettra-Sincrotrone (Trieste, Italy). Parallel SAXS and WAXS spectra can be measured during a calorimetric scan, thanks to a custom DSC instrument. Multilamellar solutions were put in calibrated glass capillaries (WJM-Glas, De) with 1.5 mm diameter and submitted to identical temperature cycles in the temperature range 25 °C < T < 55 °C at a scan rate of 1 °C/min. Several short frames were acquired for 5 s and summed up, after checking for radiation damage. The scattered radiation was angularly regrouped after normalization and background subtraction in a wide q region (0.1 < q < 20 nm-1) allowing for structural investigation of membranes on a wide length-scale.

Neutron scattering experiments. Neutron scattering measurements were performed on the thermal (λ = 2.23 Å) high-energy

resolution backscattering spectrometer IN13 (Institut Laue-Langevin, Grenoble, France). Experimental details are reported in the Supplementary Material.

The experimental data consist of the elastic neutron scattering intensity S(Q, ω = 0) vs. the squared momentum transfer (Figure S2). In the low Q region the Q-dependence of S(Q, ω = 0) is given, according to the Gaussian approximation, by:

$$S(Q,\omega=0) = I_0 e^{-\frac{\langle u^2\rangle Q^2}{6}} \quad (1)$$

where I_0 is a constant and $\langle u^2 \rangle$ is the mean-square amplitude of atomic displacements (MSD).

Thus, from the slope of the semi-logarithmic plot of the incoherent scattering function, the Mean Square Displacements (MSD) for a given T is extracted.

The temperature variation of the MSDs can be interpreted in terms of an *empirical effective force constant* called $\langle k' \rangle$, called *resilience* by Zaccai [37]. It describes the rigidity or resilience of the macromolecules. The effective average force constant for sample dynamics, $\langle k' \rangle$, can then be calculated from the slope of MSD as a function of temperature, by applying a quasi-harmonic approximation:

$$\langle k' \rangle = 0.00276/[(d\langle u2 \rangle) / dT] \quad (2)$$

MD simulations parameters. All the molecular dynamics simulations of this work were performed with the Gromacs software package (version 2020)[47] in the NpT ensemble, with periodic boundary conditions in all dimensions. We used the OPLS-UA force field [31] combined with Berger lipids [32], as done in previous works [15,48]. We used a leap-frog integrator with a time step of 2 fs. For production runs of square systems at 57 °C, we used the Parrinello-Rahman barostat [49] (with 1 ps of relaxation time) to apply semi-isotropic pressure scaling and keep the pressure at 1 bar, while using the velocity rescale [50] algorithm (with a time constant of 1 ps) to keep the temperature constant. The systems used for the unbiased simulations of Fig. 3 and the calculation of bending modulus contained 880 DPPC molecules organized in simulation boxes with a square xy plane (dimensions ranging from ~17 × 17 nm to ~18.5 × 18.5 nm depending on the PS chains mass ratio). The systems used for the simulations of Fig. 4 contained 1100 DPPC molecules organized in simulation boxes with a rectangular xy plane (~7.5 × 38 nm).

Calculation of bending modulus. The membrane bending modulus, K_b, was calculated via the analysis of membrane buckling, as recently proposed by Deserno [51] and reviewed in Bochicchio et al. [52]. The DPPC bilayers were buckled by applying a pressure in the x-direction until a strain of around 0.2 was reached (the y edge of the simulation box was fixed during the compression). Then, 1-microsecond simulations were carried out with constant x and y box dimensions. The value of the xx element of the stress tensor was then used to derive the force exerted by the membrane in the x-direction, which is related to K_b [51]. Only the last 500 ns were used for averaging.

Order parameter θ. We designed an order parameter (called θ) to discriminate between ordered and disordered DPPC lipid tails while being independent of the local membrane normal. For each lipid tail in each leaflet, we calculate the absolute value of all its dihedrals (IUPAC convention, 0 rad corresponding to perfect *cis*-conformation), we select the smallest of these values, and we assign a value of θ = 0 if it is < 2 rad and of θ = 1 if it is >= 2 rad. Then we divide the xy plane in a grid, and we average all the θ values of each bin. This procedure produces a 2D map for a single frame. To have statistically meaningful results, we averaged the grids obtained from 10 ns of simulation after 500 ns of equilibration.

Author contributions

GR and EDF conceived the study. EDF, LC, LP, MVC performed DSC and SAXS experiments and analyzed the data. LC, EDF and FN performed the ENS experiments and analyzed the data. GR, LM and DB planned the computational work, and DB performed all the simulations. GR, DB, EDF, LC and LM wrote the paper.

Declaration of Competing Interest

The authors declare that they have no known competing financial interests or personal relationships that could have appeared to influence the work reported in this paper.

Acknowledgements

GR acknowledges funding from the ERC Starting Grant BioMNP 677513. GR and DB acknowledge funding for computational resources from MIUR – DIFI, Dipartimento di Eccellenza 2018-2022. EDF thanks the Department of Medical Biotechnologies and Translational Medicine of the Università degli Studi di Milano for grant PSR 2019 to EDF. The authors acknowledge CERIC-ERIC proposal grant n. 20192174 and the staff at the SAXS beamline (Elettra Sincrotrone, Trieste). The authors acknowledge ILL proposal grant (9-13-917) to perform neutron scattering experiments (10.5291/ILL-DATA.9-13-917) and the staff at the IN13 neutron beamline (ILL, Grenoble) for technical assistance. LM acknowledges funding from the Institut national de la santé et de la recherche médicale (INSERM).

Appendix A. Supplementary material

Supplementary data to this article can be found online at https://doi.org/10.1016/j.jcis.2021.07.069.

References

[1] J. Brahney, M. Hallerud, E. Heim, M. Hahnenberger, S. Sukumaran, Plastic rain in protected areas of the United States, Science. 368 (6496) (2020) 1257–1260, https://doi.org/10.1126/science:aaz5819.
[2] C.J. Moore, Synthetic polymers in the marine environment: A rapidly increasing, long-term threat, Environ. Res. 108 (2) (2008) 131–139, https://doi.org/10.1016/j.envres.2008.07.025.
[3] B. Gewert, M.M. Plassmann, M. MacLeod, Pathways for degradation of plastic polymers floating in the marine environment, Environ. Sci. Process. Impacts 17 (9) (2015) 1513–1521, https://doi.org/10.1039/C5EM00207A.
[4] A.L. Andrady, Microplastics in the marine environment, Mar. Pollut. Bull. 62 (8) (2011) 1596–1605, https://doi.org/10.1016/j.marpolbul.2011.05.030.
[5] M. Cole, P. Lindeque, C. Halsband, T.S. Galloway, Microplastics as contaminants in the marine environment: a review, Mar. Pollut. Bull. 62 (12) (2011) 2588–2597, https://doi.org/10.1016/j.marpolbul.2011.09.025.
[6] M.C. Fossi, C. Panti, C. Guerranti, D. Coppola, M. Giannetti, L. Marsili, R. Minutoli, Are baleen whales exposed to the threat of microplastics? A case study of the Mediterranean fin whale (Balaenoptera physalus), Mar. Pollut. Bull. 64 (11) (2012) 2374–2379, https://doi.org/10.1016/j.marpolbul.2012.08.013.
[7] M.T. Ekvall, M. Lundqvist, E. Kelpsiene, E. Šileikis, S.B. Gunnarsson, T. Cedervall, Nanoplastics formed during the mechanical breakdown of daily-use polystyrene products, Nanoscale Adv. 1 (3) (2019) 1055–1061, https://doi.org/10.1039/C8NA00210J.
[8] Z. Pilevar, A. Bahrami, S. Beikzadeh, H. Hosseini, S.M. Jafari, Migration of styrene monomer from polystyrene packaging materials into foods: characterization and safety evaluation, Trends Food Sci. Technol. 91 (2019) 248–261, https://doi.org/10.1016/j.tifs.2019.07.020.
[9] M.A. Browne, A. Dissanayake, T.S. Galloway, D.M. Lowe, R.C. Thompson, Ingested microscopic plastic translocates to the circulatory system of the mussel, Mytilus edulis (L), Environ. Sci. Technol. 42 (13) (2008) 5026–5031.
[10] C.M. Boerger, G.L. Lattin, S.L. Moore, C.J. Moore, Plastic ingestion by planktivorous fishes in the North Pacific Central Gyre, Mar. Pollut. Bull. 60 (12) (2010) 2275–2278, https://doi.org/10.1016/j.marpolbul.2010.08.007.
[11] K. Kik, B. Bukowska, P. Sicińska, Polystyrene nanoparticles: Sources, occurrence in the environment, distribution in tissues, accumulation and toxicity to various organisms, Environ. Pollut. 262 (2020) 114297, https://doi.org/10.1016/j.envpol.2020.114297.

[12] B.G. Kwon, K. Koizumi, S.Y. Chung, Y. Kodera, J.O. Kim, K. Saido, Global styrene oligomers monitoring as new chemical contamination from polystyrene plastic marine pollution, J. Hazard. Mater. 300 (2015) 359–367, https://doi.org/10.1016/j.jhazmat.2015.07.039.
[13] T. Altares, D.P. Wyman, V.R. Allen, Synthesis of low molecular weight polystyrene by anionic techniques and intrinsic viscosity–molecular weight relations over a broad range in molecular weight, J. Polym. Sci. Part A Gen. Pap. 2 (1964) 4533–4544, https://doi.org/10.1002/pol.1964.100021021.
[14] D.J. Plazek, V.M. O'Rourke, Viscoelastic behavior of low molecular weight polystyrene, J. Polym. Sci. Part A-2 Polym. Phys. 9 (1971) 209–243, https://doi.org/10.1002/pol.1971.160090202.
[15] G. Rossi, J. Barnoud, L. Monticelli, Polystyrene Nanoparticles Perturb Lipid Membranes, J. Phys. Chem. Lett. 5 (1) (2014) 241–246, https://doi.org/10.1021/jz402234c.
[16] D. Bochicchio, E. Panizon, L. Monticelli, G. Rossi, Interaction of hydrophobic polymers with model lipid bilayers, Sci. Rep. 7 (1) (2017), https://doi.org/10.1038/s41598-017-06668-0.
[17] S.J. Marrink, A.H. de Vries, A.E. Mark, Coarse Grained Model for Semiquantitative Lipid Simulations, J. Phys. Chem. B 108 (2) (2004) 750–760, https://doi.org/10.1021/jp036508g.
[18] M. Jung, D.H.W. Hubert, E. van Veldhoven, P.M. Frederik, M.J. Blandamer, B. Briggs, A.J.W.G. Visser, A.M. van Herk, A.L. German, Interaction of styrene with DODAB bilayer vesicles. Influence on vesicle morphology and bilayer properties, Langmuir 16 (3) (2000) 968–979, https://doi.org/10.1021/la990698y.
[19] M.I. Morandi, M. Kluzek, J. Wolff, A. Schroder, F. Thalmann, C.M. Marques, Accumulation of styrene oligomers alters lipid membrane phase order and miscibility, Proc. Natl. Acad. Sci. USA 118 (2021) 1–7, https://doi.org/10.1073/pnas.2016037118.
[20] A. Aroti, E. Leontidis, M. Dubois, T. Zemb, Effects of monovalent anions of the Hofmeister series on DPPC lipid bilayers part I: Swelling and in-plane equations of state, Biophys. J. 93 (5) (2007) 1580–1590, https://doi.org/10.1529/biophysj.106.094482.
[21] J.M. Sturtevant, Biochemical applications of differential scanning calorimetry, Annu. Rev. Phys. Chem. 38 (1) (1987) 463–488, https://doi.org/10.1146/annurev.pc.38.100187.002335.
[22] T. Heimburg, A model for the lipid pretransition: coupling of ripple formation with the chain-melting transition, Biophys. J. 78 (3) (2000) 1154–1165, https://doi.org/10.1016/S0006-3495(00)76673-2.
[23] M. Rappolt, G. Pabst, G. Rapp, M. Kriechbaum, H. Amenitsch, C. Krenn, S. Bernstorff, P. Laggner, New evidence for gel-liquid crystalline phase coexistence in the ripple phase of phosphatidylcholines, Eur. Biophys. J. 29 (2) (2000) 125–133, https://doi.org/10.1007/s002490050257.
[24] J. Katsaras, S. Tristram-Nagle, Y. Liu, R.L. Headrick, E. Fontes, P.C. Mason, J.F. Nagle, Clarification of the ripple phase of lecithin bilayers using fully hydrated, aligned samples, Phys. Rev. E - Stat. Physics, Plasmas, Fluids, Relat. Interdiscip. Top. 61 (5) (2000) 5668–5677, https://doi.org/10.1103/PhysRevE.61.5668.
[25] J.F. Nagle, P. Cognet, F.G. Dupuy, S. Tristram-Nagle, Structure of gel phase DPPC determined by X-ray diffraction, Chem. Phys. Lipids. 218 (2019) 168–177, https://doi.org/10.1016/j.chemphyslip.2018.12.011.
[26] W.-J. Sun, R.M. Suter, M.A. Knewtson, C.R. Worthington, S. Tristram-Nagle, R. Zhang, J.F. Nagle, Order and disorder in fully hydrated unoriented bilayers of gel-phase dipalmitoylphosphatidylcholine, Phys. Rev. E 49 (5) (1994) 4665–4676, https://doi.org/10.1103/PhysRevE.49.4665.
[27] T.T. Mills, G.E.S. Toombes, S. Tristram-Nagle, D.-M. Smilgies, G.W. Feigenson, J. F. Nagle, Order parameters and areas in fluid-phase oriented lipid membranes using wide angle x-ray scattering, Biophys. J. 95 (2) (2008) 669–681, https://doi.org/10.1529/biophysj.107.127845.
[28] H. Yao, S. Matuoka, B. Tenchov, I. Hatta, Metastable ripple phase of fully hydrated dipalmitoylphosphatidylcholine as studied by small angle x-ray scattering, Biophys. J. 59 (1) (1991) 252–255, https://doi.org/10.1016/S0006-3495(91)82216-0.
[29] K. Akabori, J.F. Nagle, Structure of the DMPC lipid bilayer ripple phase, Soft Matter 11 (5) (2015) 918–926, https://doi.org/10.1039/C4SM02335H.
[30] A.H. de Vries, S. Yefimov, A.E. Mark, S.J. Marrink, Molecular structure of the lecithin ripple phase, Proc. Natl. Acad. Sci. USA 102 (15) (2005) 5392–5396, https://doi.org/10.1073/pnas.0408249102.
[31] W.L. Jorgensen, J.D. Madura, C.J. Swenson, Optimized intermolecular potential functions for liquid hydrocarbons, J. Am. Chem. Soc. 106 (22) (1984) 6638–6646.
[32] O. Berger, O. Edholm, F. Jähnig, Molecular dynamics simulations of a fluid bilayer of dipalmitoylphosphatidylcholine at full hydration, constant pressure, and constant temperature, Biophys. J. 72 (5) (1997) 2002–2013, https://doi.org/10.1016/S0006-3495(97)78845-3.
[33] V. Zoni, V. Nieto, L.J. Endter, H.J. Risselada, L. Monticelli, S. Vanni, To bud or not to bud: a perspective on molecular simulations of lipid droplet budding, Front. Mol. Biosci. 6 (2019) 2017–2020, https://doi.org/10.3389/fmolb.2019.00124.
[34] A.R. Thiam, E. Ikonen, Lipid droplet nucleation, Trends Cell Biol. 31 (2) (2021) 108–118, https://doi.org/10.1016/j.tcb.2020.11.006.
[35] V. Choudhary, N. Ojha, A. Golden, W.A. Prinz, A conserved family of proteins facilitates nascent lipid droplet budding from the ER, J. Cell Biol. 211 (2015) 261–271, https://doi.org/10.1083/jcb.201505067.
[36] H. Pfeiffer, H. Binder, G. Klose, K. Heremans, Hydration pressure and phase transitions of phospholipids: II. Thermotropic approach, Biochim. Biophys. Acta - Biomembr. 1609 (2) (2003) 148–152, https://doi.org/10.1016/S0005-2736(02)00665-X.
[37] G. Zaccai, How soft is a protein? A protein dynamics force constant measured by neutron scattering, Science (80-) 288 (2000) 1604–1607, https://doi.org/10.1126/science.288.5471.1604.
[38] R. Goetz, G. Gompper, R. Lipowsky, Mobility and elasticity of self-assembled membranes, Phys. Rev. Lett. 82 (1) (1999) 221–224, https://doi.org/10.1103/PhysRevLett.82.221.
[39] J. Eid, H. Razmazma, A. Jraij, A. Ebrahimi, L. Monticelli, On calculating the bending modulus of lipid bilayer membranes from buckling simulations, J. Phys. Chem. B 124 (29) (2020) 6299–6311, https://doi.org/10.1021/acs.jpcb.0c04253.
[40] E.G. Kelley, P.D. Butler, R. Ashkar, R. Bradbury, M. Nagao, Scaling relationships for the elastic moduli and viscosity of mixed lipid membranes, Proc. Natl. Acad. Sci. USA 117 (38) (2020) 23365–23373, https://doi.org/10.1073/pnas.2008789117.
[41] J.F. Nagle, Experimentally determined tilt and bending moduli of single-component lipid bilayers, Chem. Phys. Lipids 205 (2017) 18–24, https://doi.org/10.1016/j.chemphyslip.2017.04.006.
[42] P.C. Ke, S. Lin, W.J. Parak, T.P. Davis, F. Caruso, A decade of the protein corona, ACS Nano 11 (12) (2017) 11773–11776, https://doi.org/10.1021/acsnano.7b08008.
[43] S. Lin, M. Mortimer, R. Chen, A. Kakinen, J.E. Riviere, T.P. Davis, F. Ding, P.C. Ke, NanoEHS beyond toxicity-focusing on biocorona, Environ. Sci. Nano. 4 (7) (2017) 1433–1454, https://doi.org/10.1039/C6EN00579A.
[44] R.S. Cantor, Lateral pressures in cell membranes: a mechanism for modulation of protein function, J. Phys. Chem. B 101 (1997) 1723–1725, https://doi.org/10.1021/jp963911x.
[45] O.H.S. Ollila, H.J. Risselada, M. Louhivuori, E. Lindahl, I. Vattulainen, S.J. Marrink, 3D Pressure field in lipid membranes and membrane-protein complexes, Phys. Rev. Lett. 102 (2009), https://doi.org/10.1103/PhysRevLett.102.078101 078101.
[46] G. Salvetti, C. Cardelli, C. Ferrari, E. Tombari, A modulated adiabatic scanning calorimeter (MASC), Thermochim. Acta 364 (1-2) (2000) 11–22, https://doi.org/10.1016/S0040-6031(00)00645-6.
[47] M.J. Abraham, T. Murtola, R. Schulz, S. Páll, J.C. Smith, B. Hess, E. Lindahl, High performance molecular simulations through multi-level parallelism from laptops to supercomputers, SoftwareX 1-2 (2015) 19–25, https://doi.org/10.1016/j.softx.2015.06.001.
[48] E. Panizon, D. Bochicchio, L. Monticelli, G. Rossi, MARTINI coarse-grained models of polyethylene and polypropylene, J. Phys. Chem. B 119 (25) (2015) 8209–8216, https://doi.org/10.1021/acs.jpcb.5b03611.
[49] M. Parrinello, A. Rahman, Polymorphic transitions in single crystals: a new molecular dynamics method, J. Appl. Phys. 52 (1981) 7182.
[50] G. Bussi, D. Donadio, M. Parrinello, Canonical sampling through velocity rescaling, J. Chem. Phys. 126 (1) (2007) 014101, https://doi.org/10.1063/1.2408420.
[51] M. Hu, P. Diggins IV, M. Deserno, Determining the bending modulus of a lipid membrane by simulating buckling, J. Chem. Phys. 138 (2013) 1–13, https://doi.org/10.1063/1.4808077.
[52] D. Bochicchio, L. Monticelli, Chapter five – the membrane bending modulus in experiments and simulations: a puzzling picture, Adv. Biomembr. Lipid Self-Assembly 23 (2016) 117–143, https://doi.org/10.1016/bs.abl.2016.01.003.